Master of Science Thesis in
Medical Radiation Physics

Improved analysis of MRI tractography data: Group comparisons of parameters along fibre tracks

Johanna Mårtensson

Supervisors: Jimmy Lätt and Markus Nilsson
Medical Radiation Physics
Department of Clinical Sciences, Lund University
Lund, Sweden
2010

Contents

Abstract

Diffusion MRI is an imaging technique capable of inferring information about the tissue microstructure, based on magnetic resonance imaging (MRI). Diffusion MRI data can be analysed using tractography, a tool able to represent the structure of the white matter (WM) in the brain. Tractography is commonly used qualitatively, but in this report, an algorithm for quantitative tractography was developed.

A new evaluation method was developed in order to analyse diffusion parameters in all positions along WM pathways. The developed algorithm was then applied to WM pathways that had been calculated and extracted in a software, based on streamline tractography calculations of the diffusion data. Co-registrations of the data made comparisons across subjects and between groups possible. The algorithm was tested by analysing the inferior-fronto occipital fasciculus (IFO) in males versus females as well as young versus old healthy volunteers. Comparisons were also performed to clinical research projects, by analyzing the IFO in semantic dementia (SD) patients versus healthy controls (HC-SD) and the inferior longitudinal fasciculus (IFL) in intrauterine growth restriction (IUGR) patients versus HC-IUGR.

The calculated values of the diffusion parameters were in agreement with was expected from earlier published results. In the SD patients, diffusion parameters were significant different from the parameters in HC-SD in anterior as well as in posterior parts of the IFO. Large regions of significant differences were present the temporal lobe, when diffusion parameters of the IFL were compared between IUGR patients and HC-IUGR.

In summary, with the aid of an in-house developed algorithm, diffusion parameters could be calculated along the WM pathways. This new evaluation method could lead to a higher sensitivity in detecting local deviations in the properties of the WM pathways, as compared to what could be achieved with conventional analysis methods.

Abbreviations

AAC	Apparent area coefficient
AD	Alzeimer´s disease
ADC	Apparent diffusion coefficient
aMCI	amnestic Mild cognitive impairment
DT	Diffusion tensor
DTI	Diffusion tensor imaging
DTT	Diffusion tensor tractography
DW-MRI	Diffusion weighted magnetic resonance imaging
EPI	Echo planar imaging
F	Female
FA	Fractional anisotropy
FOV	Field of view
FSL-FLIRT	FMRIB Software Library - FMRIB's Linear Image Registration Tool (linear inter- and intra-modal registration)
FTD	Frontotemporal dementia
GM	Grey matter
HC	Healthy controls
HC-IUGR	Healthy controls Intra uterine growth restriction
HC-SD	Healthy controls semantic dementia
IFL	Inferior longitudinal fasciculus
IFO	Inferior fronto-occipital fasciculus
IUGR	Intrauterine growth restriction
M	Male
MD	Mean diffusivity
MRI	Magnetic resonance imaging
MS	Multiple Sclerosis
O	Old
ODF	Orientation distribution functions
OFC	Orbitofrontal cortex
QBI	Q-ball imaging
ROI	Region of interest
SD	Semantic dementia
SFO	Superior fronto-occipital fasciculus
SSSE	Single shot spin echo
TE	Time of echo
TR	Time of repetition
WM	White matter
Y	Young

Symbols

b	diffusion weightning factor
D	Diffusion coefficient
λ_1	Eigenvalue in the predominal direction
λ_2	Second eigenvalue
λ_3	Third eigenvalue
t_D	Time of diffusion
x_{rms}	Root mean square distance

1. Introduction

Magnetic resonance imaging (MRI) is an important imaging technique that is essential in modern diagnostic radiology. MRI produces morphological images of the soft tissue with high contrast, which is, for instance, not possible with computed tomography. Furthermore, MRI facilitates the study of the function of several organs. For example, the connectivity of the white matter (WM) between different brain regions can be studied with diffusion tensor imaging (DTI) and diffusion tensor tractography (DTT). In this report, a quantitative method for analysing diffusion properties along WM pathways, based on DTT, is described.

1.1 Diffusion and tractography in MRI

Diffusion weighted magnetic resonance imaging (DW-MRI) is an imaging technique, based on measurements of the translational random motion effects of water molecules [1]. This process is affected by the tissue microstructure and thereby the obtained image intensity is an indirect measure of the tissue microstructure [2]. For instance, when the molecular motion is hindered in a spatial direction, also the measured diffusivity in that direction is reduced [3]. Since the nerve fibres are composed as bundles of axons, covered by cylindrical myelin sheaths that restrict the diffusion, the diffusivity perpendicular to the nerve fibres is severely reduced as compared to the diffusivity parallel to the axons [4].

DTI is a technique for estimating the predominal diffusion direction of water in each image voxel [5,6]. By performing DTT, i.e. connecting the preferred diffusion direction in an image voxel with the predominal diffusion directions in adjacent image voxels, a 3D map of the cerebral nerve system can be obtained [6,7,8]. By limiting the voxels included in the analysis, it is possible to extract individual WM pathways and visualise them according to Figure 1 [7,6]. The WM of the brain is subdivided into different pathways, based on anatomical and functional criteria [8,9]. The nerve fibres in these WM pathways connect different regions in the brain to each other. In the following text, a nerve fibre bundle composing a pathway in the brain is denoted a WM pathway, while the mathematical representation of the nerve fibres in a WM pathway are denoted tracks. These definitions may differ in different publications.

1.2 Diffusion in the white matter of human brain

The diffusivities perpendicular and parallel to the nerve fibres are affected by several neurological diseases. In the case of demyelination, i.e. a degeneration of the myelin and thus of the barriers around the axons, the diffusivity perpendicular to the nerve fibres increases [10]. A reduced diffusivity along the nerves, on the other hand, could be caused by degenerative changes in the micro structural integrity of the WM [11]. Axonal loss or destruction of myelin sheaths can also be a result of degenerative WM disorders, e.g. multiple sclerosis (MS) [12,13] and varieties of dementia [**Error! Bookmark not defined.**14]. The progression of such diseases is assessable using the fractional anisotropy (FA), a metric calculated from the diffusion tensor reflecting the WM integrity [11,10]. Studies have also shown that after the middle age, the FA in the WM decrease with age [15], likely due to the demyelisation that occurs naturally in the ageing brain [15,16]. Another possible cause of a decreased FA is an increasing amount of crossing nerve fibres with age, i.e. more axons going in a direction perpendicular to the direction of the main nerve fibre [17].

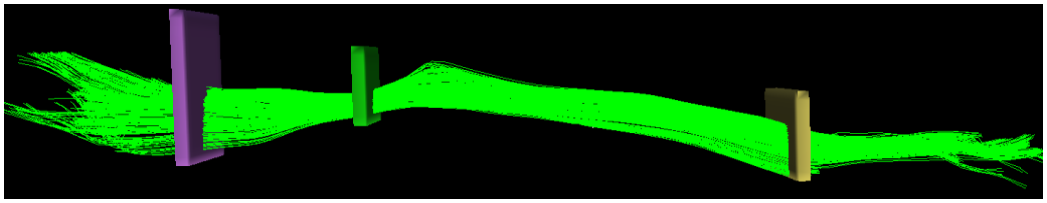

Figure 1 A reconstructed bundle of tracks representing a WM pathway is shown. In this figure, tracks connecting the frontal and occipital lobes were selected using three coronal ROIs, shown by rectangular boxes. Every green line in the bundle corresponds to a calculated track.

1.3 Qualitative versus quantified DTT

Tractography is often used qualitatively, i.e. the extent and shape of track bundles are used to interpret functional deficits [18]. For example, tractography is employed in pre-surgical tumour characterisation, in order to investigate whether the tumour has infiltrated or dislocated the surrounding tissue [19]. The quantitative potential of DTT, however, has so far not been fully explored [20]. In commonly employed analysis methods, the average values of diffusion properties in the voxels within the tracks representing a WM pathway are extracted and compared between, for instance, a group of patients and healthy controls (HC). Those average values are, however, not sensitive in detecting effects differences in diffusion properties in limited regions of the WM pathways. For instance, no significant differences in diffusion properties were found between patients suffering from Alzeimer´s diseases (AD) and HC, or between patients with amnestic Mild Cognitive Impairment (aMCI) and HC, when compared using the average values of the voxels in the tracks representing the inferior fronto-occipital fasciculus (IFO) [21].

In patients suffering from frontotemporal dementia (FTD), with defective cognitive processing and decision making, it is of interest to study the degree of degeneration in the frontal lobe of the brain [22]. The IFO is a WM pathway connecting the orbitofrontal cortex (OFC), which is an area in the anterior part of the frontal lobe, with the primary ventral cortex in the occipital lobe [24,23]. However, functions of the IFO are poorly understood, even though it is of major interest in dementia research, since the IFO might be important for semantic processing and possibly the IFO might be able to compensate degeneration of the the inferior longitudinal fasciculus (IFL) [24].

The IFL is another WM pathway, of interest to study in patients suffering from intrauterine growth restriction (IUGR) [24]. This WM pathway connects the temporal lobe to the primary ventral cortex [23,24]. The IFL is important for the functions of visual perceptions, visual memory, reading and language [23,24]. IUGR patients, who have been growth inhibited in uterus and born too early, will likely suffer from neurological and cognitive symptoms later in life [25,41]. These symptoms could possibly be correlated to degenerations in the IFL [25].

The background to the investigations described in the present work was an interest from researchers in Lund to study these pathways using tractography. An improved quantitative method was required, since previously employed methods were not sensitive to small regional differences of diffusion properties in the pathways between groups of patients and HC.

1.4 Previous studies

Clinical diffusion measurements have their beginning in the 1980's when Le Bihan *et al.* found differences in the values of the apparent diffusion coefficient (ADC) between normal and pathological tissues [26]. The application of diffusion measurements got into progress in 1990 when Moseley *et al.* demonstrated an ADC map of an ischemic lesion in cat brain, processed within an hour after onset [27]. This was the first time one was able to depict an

ischemic lesion within hours from the onset, before it became visible in conventional medical images. The concept of tractography was introduced as MR diffusion tensor imaging by Basser *et al.* in 1994 [28].

Methods for analysing diffusion parameters along the tracks have been described previously. For instance, Gerig *et al.* applied DTT to reconstruct WM tracks and calculated diffusion properties within track bundle cross-sections along track bundles [20]. However, the tracking in this method was not guided by geometric constraints, which increased the risk of including tracks from WM pathways other than the intended into the analysis. As an improvement, Fillard *et al.* manually applied an anatomical landmark in the centre of the tracks and calculated diffusion parameters as a function of the distance from the landmark [29]. The use of a single landmark could, however, reduce the accuracy in group comparisons, since the length of WM pathways may differ between individuals. Partridge *et al.* performed DTT in premature newborn, in order to quantify diffusion properties of the pyramidal tracks in WM [30]. A special tracking algorithm was developed, but its application focused on the pyramidal tracks. Klein *et al.* proposed a clustering method for robust and reproducible quantification of diffusion parameters along track bundles, although the clustering process was performed without using the underlying anatomy as an input [31].

None of these studies considered the spatial extent of WM tracks, and the methods were tested neither for the IFO nor for the IFL. These WM pathways are of interest, for example, when studying degenerative disorders that affect cognitive and neurological abilities. Moreover, the IFO and the IFL differ in spatial distribution from the WM pathways included in the studies mentioned above. None of the studies performed a track bundle normalisation with the aid of more than one anatomical landmark, which is important when comparing diffusion properties between subjects.

The aim of this work was to increase the sensitivity of tractography in detecting regional differences of diffusion properties along WM pathways between groups. An algorithm was therefore developed and its application was tested to compare the diffusion properties in male versus female (M vs F) and young versus old (Y vs O) groups of healthy volunteers. The feasibility of the method was tested using DTI data obtained from two patient groups, i.e. one group of semantic dementia (SD) patients and one with patients suffering from intrauterine growth restriction (IUGR).

2. Theory

2.1 Diffusion basics

Random translational motion of molecules or ions is caused by internal kinetic energy and called Brownian motion [32]. The amount of diffusion can be expressed in terms of a diffusion coefficient (D), which is dependent on the size of the molecules, the surrounding medium and the temperature [33]. The root mean square distance (x_{rms}) of the translational displacements during a diffusion time (t_D), can be calculated by Einstein's diffusion equation according to

$$x_{rms} = \sqrt{2Dt_D} \tag{1}$$

2.2 The diffusion tensor

In the case of free diffusion, the displacement probability of the water molecules is equal in all directions. This can be described by a sphere, where the surface represents the isobar surface of the displacement probability distribution. For isotropic free diffusion, the displacements of the water molecules follow a Gaussian distribution.

If barriers limit the molecular movement in any direction, the diffusion becomes hindered. In the case of cylindrical barriers, the isobar surface of the displacement probability distribution will no longer be spherical. A scalar D is then not sufficient to describe the diffusion, and therefore the concept of a diffusion tensor is introduced. For instance, diffusion in a hollow tube can be approximated using a diffusion tensor **DT**, where the isosurface of the displacement distribution will be shaped as an ellipsoid. The direction with highest diffusion rate, i.e. the predominal direction, is given by the largest eigenvalue, describing the ellipsoid. Mathematically, the **DT** is a rank-two tensor, given by

$$\mathbf{DT} = \begin{bmatrix} D_{xx} & D_{xy} & D_{xz} \\ D_{yx} & D_{yy} & D_{yz} \\ D_{zx} & D_{zy} & D_{zz} \end{bmatrix} \tag{2}$$

where the isosurface of displacement distribution corresponds to the nine matrix elements and from there can be used to describe the shape of the **DT**. The three eigenvalues of the diffusion tensor (λ_1, λ_2, λ_3) are obtained after diagonalisation of the **DT** and describe the diffusion rate along the principal axes of the ellipsoid. λ_1 corresponds to the predominal direction while λ_2 and λ_3 corresponds to the remaining directions and are consequently described by the shorter ellipsoid axes, see Figure 2. Even though the **DT** is defined by nine coefficients, it is sufficient to describe it by only six coefficients, because the tensor is rotationally invariant, i.e. $D_{xy} = D_{yx}$.

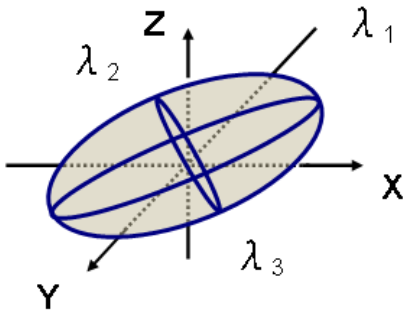

Figure 2 A principal sketch of a diffusion ellipsoid in the image coordinate system x, y and z. The principal axes of the ellispoid corresponding to its eigenvalues. λ_1 describes diffusion in the predominal direction while λ_2 and λ_3 describes diffusion in the other directions.

2.3 Mean diffusivity and fractional anisotrophy

Two metrics are commonly calculated from the **DT**; the average diffusion rate in all directions denoted the mean diffusivity (MD), and the fractional anisotropy (FA). The MD is defined as the average of the eigenvalues, according to the trace (Tr) of the **DT** divided by the number of dimensions, i.e. 3.

$$\mathrm{MD} = \mathrm{Tr}(\mathbf{DT})/3 \tag{3}$$

where Tr(**DT**) is the trace of the tensor. Furthermore, the FA is in the range 0 to 1 and derived from the standard deviations of the three eigenvalues defined as mean value of the standard deviation in the three eigenvalues according to

$$FA = \left(\frac{3}{2}\right)^{1/2} \left(\frac{(\lambda_1 - MD)^2 + (\lambda_2 - MD)^2 + (\lambda_3 - MD)^2}{(\lambda_1 + \lambda_2 + \lambda_3)^{1/2}} \right)^{1/2} \tag{4}$$

In other words, the FA is a dimensionless parameter, describing the degree of anisotropic diffusion. Isotropic diffusion would give a FA value of zero while completely directional diffusion ($\lambda_1 > 0$, $\lambda_2 = \lambda_3 \sim 0$) would give a FA value of unity. In the brain, the FA values depend on the microstructure of axonal cell membranes and myelin sheaths. Higher FA values are observed in WM pathways, where the axons are highly ordered and myelinated. In the grey matter (GM), the microstructure is less ordered.

2.4 Brain anatomy

WM is a part of the central nervous system and consists mostly of myelinated axons, with a typical diameter of 1 to 10 µm [34]. WM can be divided into different WM pathways, which consists of several individual nerve fibres, connecting to different regions of the brain [35].

An important constituent of WM is myelin, which is an outgrowth of glial cells. It forms myelin sheaths around the axons, which can be seen in the principal drawing of a neuron in Figure 3, and it increases the propagation velocity of impulses along the nerve fibres. The myelin sheaths also act like barriers to the diffusion of water, making the diffusion highly anisotropic [36]. The structure of a myelin sheath can be visualised using electron microscopy, see Figure 4.

The FA is sensitive to the progression of degenerative WM disorders resulting in axonal losses or destruction of the myelin sheaths [37]. Examples of this type of disorders are MS and various kinds of dementia [37]. Results have shown that the FA values decrease with age due to demyelination [38], which befalls naturally in the middle age.

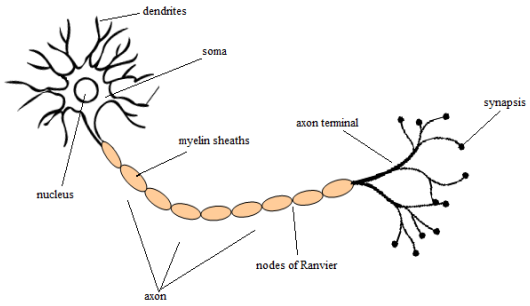

Figure 3 Principal drawing of a neuron. The axon is surrounded by myelin sheaths that are separated by the nodes of Ranvier. The soma contains the nucleus and is located in one of the ends, with dendrites spread out in the surrounding tissue. Communications with target neurons occurs in the synapses placed in the axon terminals.

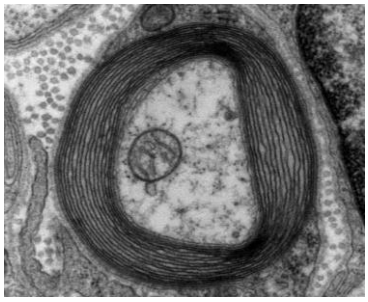

Figure 4 Cross-section of a myelinated axon, visualised in electron microscopy. The image has been generated at the Electron Microscopy Facility at Trinity College, Hartford, CT, and was obtained from Wikipedia.

The human brain is divided into several lobes, and these can be further divided into physiological areas. One of the lobes is the frontal lobe which is located directly behind the forehead. The frontal lobe contains the largest amount of neurons that are sensitive to dopamine, which limits and selects sensory information sent from thalamus. Executive functions of frontal lobe are the ability to recognize consequences from actions, to make decisions and modify emotions to fit social acceptable norms [39].

The occipital lobe is located in the back of the head and contains most parts of the visual cortex, such as the primary visual cortex, located on the medial side of the lobe and the visual processing centre, subdivided into several functional visual regions.

The temporal lobe is located beneath the Sylvian fissure and contains the hippocampus, primary auditory cortex and is involved in auditory perception. Processing of the semantic capacity for speech and vision is also located in this lobe as well as physiological functions such as naming and verbal memory [39].

In the present work, two WM pathways were of specific interest. Firstly, the WM pathway connecting OFC and the ventral part of the occipital lobe, the IFO, was analysed. The physiological function of IFO is still poorly understood, even though arguments exist about the importance of IFO for language and semantic processing [23,24]. Secondly, the IFL, which is a connection between the temporal lobe and the occipital lobe, was analysed. IFL contains long as well as short nerve fibres, where the long nerve fibres are located medial to the short ones. The physiological function of IFL is associated with face recognition and other visual perceptions, visual memory, reading and language [23]. The areas of the OFC, the temporal- and the occipital lobe can be seen in the red, green and yellow areas respectively in figure 5.

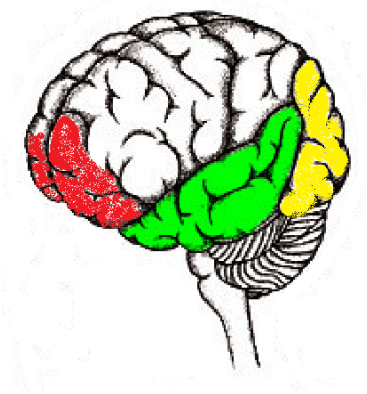

Figure 5 Sagittal slice of a human brain. The red area in the most anterior part of the frontal lobe corresponds to the OFC cortex. The green area of the brain corresponds to the temporal lobe. The yellow area in the posterior part of the brain corresponds to the occipital lobe. These are the lobes of interest when investigating the properties of IFO and IFL. The figure was originally obtained from Wikipedia.

The WM pathway of interest in SD is the IFO and in IUGR it is the IFL. SD is one of three prototypical syndromes that results from frontotemporal lobal degeneration. Patients with this progressive neurodegenerative disorder suffer from loss of semantic memory, i.e. remembering words and facts. The characteristic pattern of atrophy may appear predominantly on one specific side of the brain [40]. Intrauterine growth restriction (IUGR) is a diagnosis for fetuses with estimated weight below the 10^{th} percentile for its gestational age and whose abdominal circumference is below the 2.5^{th} percentile. Many of these children are born prematurely and the neurological development is related to the grade of prematurity and degree of growth restriction. The diagnosis can possibly affect brain growth and mental development and children diagnosed with IUGR shows a higher risk for developing deficits in attention and performance [41].

2.5 Tractography

The most commonly employed method though is the streamline tractography, which was the method performed in this work. Tractography is based on DW-MRI images, where the predominal direction of diffusion is calculated from the diffusion tensor in each voxel. A 3D map that shows the connection of the predominal diffusion directions between different voxels can then be reconstructed, see fFigure 6 **Tractography is based on information about the predominal direction, which can be obtained from the diffusion tensor and described by a diffusion ellipsoid. When the predominal direction has been calculated for each voxel, a track can be reconstructed following the principal diffusion direction, assumed to be in the nerve's direction.** .

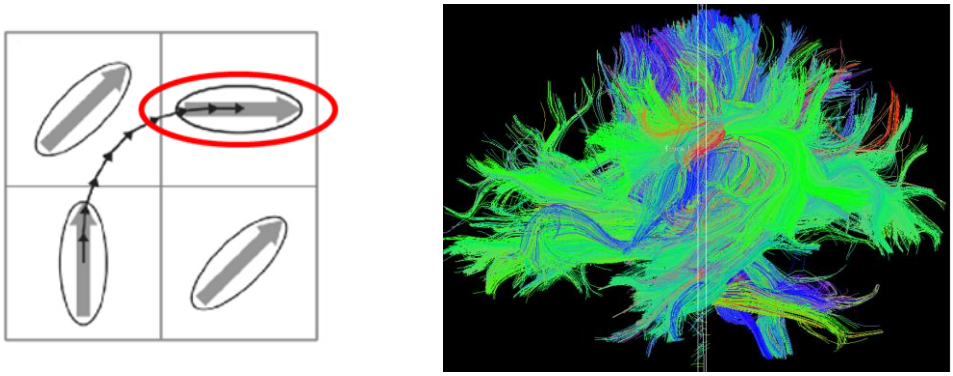

Figure 6 Tractography is based on information about the predominal direction, which can be obtained from the diffusion tensor and described by a diffusion ellipsoid. When the predominal direction has been calculated for each voxel, a track can be reconstructed following the principal diffusion direction, assumed to be in the nerve's direction. The figure to the left illustrates four voxels with calculated diffusion tensors in each voxel. As a principal sketch, the line following the tensor directions from voxel to voxel illustrates how the tractography is being calculated. To further clarify, the red ellips shows a calculated direction of the diffusion tensor. The figure to the right illustrates all calculated tracks of a brain, visualised using TrackVis.

In the present work, the streamline tractography was calculated using TrackVis [42]. All voxels with FA-values above a user-specified threshold are seeded, after which the maximum diffusion vectors are identified from the longest eigenvectors of the **DT**:s. The tracking then proceeds by performing a path computation, i.e. for each diffusion vector a path is initiated in a step of 0.5 voxels. As soon as the path enters a new voxel, the new diffusion vector is identified from the diffusion tensor, and streamlines are reconstructed. The FA values must exceed a user specified threshold in successive voxels for the tracking to continue, otherwise the track is terminated. In the present work, the threshold was specified to 0.2. Moreover, the angle of the diffusion vectors from two consecutive steps was not allowed to be above a user specified threshold specified to 45°.

3. Method

To increase the sensitivity to regional differences in diffusion properties along WM pathways between groups, a novel algorithm was developed. For each track bundle, a mean track was calculated to represent the centre of the WM pathways. Different diffusion parameters, such as MD and FA, could then be extracted in cross sections along the positions of the mean track. Comparisons of the diffusion parameters along the mean track for different volunteer and patient groups were performed in order to test the feasibility of the algorithm.

3.1 Subjects

Eight different groups of subjects were included in the comparisons, see table 1 for details. The first two group comparisons considered males versus females (M vs F) and young versus old (Y vs O). No differences in diffusion properties were expected between in the M vs F comparison, while the FA and the MD was expected to be lower and higher, respectively, in the older as compared to the younger volunteers.

In order to address questions arising from clinical research studies performed at Skåne University Hospital in Lund, another two group comparisons were performed. Diffusion properties were compared, first between SD patients and age matched SD healthy controls (SD vs HC-SD) and secondly in the IFL between IUGR patients and age matched IUGR healthy controls (HC-IUGR), see table 1. Inclusions in the control groups differed between the two group comparisons. Only volunteers without semantic and cognitive symptoms were included in the HC-SD group, i.e. the volunteers were tested for semantic and cognitive abilities by neurologists before included in the study.

Table 1. The table shows an overview of the different groups that were compared in regard to diffusion properties. From left: Groups, number of subjects, average age ± one standard deviation and finally the analysed WM pathway. HC-SD and HC-IUGR reefers to age matched control groups for SD and HC-IUGR, respectively

Compared groups	Number of subjects	Average age (y) ± 1 standard deviation	WM pathway studied
Male / Female	6 / 5	34 ± 4,1 / 36 ± 4,9	IFO
Young / Elderly	11 / 5	31 ± 2,0 / 73 ± 6,6	IFO
SD / HC-SD	4 / 7	70 ±10 / 71 ± 10	IFO
IUGR / HC-IUGR	11 / 5	24 ± 0,9 / 24 ± 0,8	IFL

3.3 Data acquisition

Measurements were performed at the Philips Achieva 3T scanner at Skåne University Hospital in Lund, Sweden. The DTI data were acquired using a single shot spin echo (SSSE) echo planar imaging (EPI) sequence with the following parameters: 60 slices, slice thickness 2 mm, field of view (FOV) 256 x 256 mm^2, voxel sixe 2x2x2 mm^3, repetition time (TR) 7881 ms, echo time (TE) 90 ms, acquisition time of 6 min 49 s and a diffusion weighting factor (*b*) of 800 s/mm^2. The measurements were performed in 48 diffusion encoding directions. Motion and eddy current correction of the data were performed using the FSL-FLIRT software, which is a tool for affine brain image registration in the FMRIB Software Library [43].

3.4 Tractography

Streamline tractography was performed using the Diffusion Toolkit and TrackVis software package, which also was used for placements of anatomical landmarks [44]. The FA threshold for the tracking was set to 0.2 and the angular threshold was 45°.

3.5 Regions of interest ROI

ROIs were applied in the parametric images in order to select and extract the WM pathways. The positioning of these was performed according to description by Mori *et al.* [45], as well as according to anatomical definitions of WM pathways described by Catani *et al.* in 2008 [45,46]. Mori *et al.* describe how to use coronar ROIs and excluding ROIs where needed while Catani *et al.* describe how to define ROIs in every slice in a region to cover the WM pathway region. A combination between these performances was used in the present work. A total of four ROIs were employed to extract the pathways, i.e. only tracks that passed through all four regions were incorporated in the following analysis.

3.5.1 Extracting the IFO

The first ROI was placed coronally in the anterior part of the brain, in the region of the external extreme capsule. The ROI was defined around its anterior floor with the insula and the lenticular nucleus used as lateral and medial borders, respectively. The most inferior slice was defined where the temporal and frontal branches of the external extreme capsule joined together. A superior border was not defined, because superior tracks did not connect to the OFC and were then excluded by the second ROI. This ROI was orientated transversally in the frontal lobe above the OFC in order to exclude tracks connecting to other frontal regions. It was positioned anterior and inferior to the ventricle. The third ROI was placed coronally in the posterior part of the brain and aimed to include tracks that connected to the ventral part of the occipital lobe. The inferior border of the ROI was defined in the lingual and fusiform gyrus. The superior border was defined where left and right splenium joined at the midsagittal line. The anterior border was defined as the tip of the occipital horn; in those cases the IFO passed posterior to this tip. For other cases the anterior limitation was individually spatially corrected. The latter limitation aimed to exclude the cingulum, which is a WM pathway that passes the tip of the occipital horn and connects thalamus and neocortex with the entorhinal cortex. When the limitation could not be fulfilled, the possibility to erroneously include cingulum in the selection consequently increased. The fourth ROI, with coronal orientation, was positioned approximately at a third of the distance between the anterior and posterior ROI in the same slices as the head of the hippocampus. Tracks originating from the IFO are anatomically required to pass through this slice [47]. This ensures the exclusion of tracks originating from the superior fronto-occipital fasciculus (SFO), which is a WM pathway that can easily be erroneously confused with IFO. The applications of the ROIs can be seen in figure 7.

Finally, one to two additional excluding ROIs were applied to exclude tracks that connected to other brain regions than the desired ones.

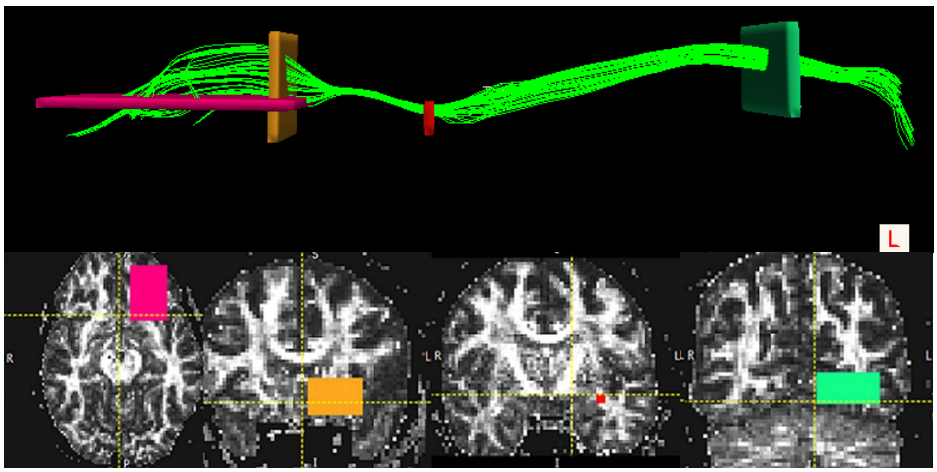

Figure 7 Application of the four ROIs for extraction of the IFO was made in a coronal orientation (A) in the frontal lobe, (B) in the occipital lobe and (C) in the major WM pathway between the frontal and occipital ROI. A transversally orientated ROI was also applied (D) in the frontal lobe in order to include only tracks from the OFC.

3.5.2 Extracting the IFL

The IFL was also extracted using four ROIs. The most anterior ROI was defined where the WM connected in the anterior part of the temporal lobe. The superior border was located three slices below the junction between the frontal and temporal branches of the anterior floor of the external capsule. The posterior ROI was oriented coronal and aimed to include tracks that connected to the ventral part of the occipital lobe. The criteria used for delineation of the occipital lobe were described in the paragraph of the IFO. Two additional ROIs, defined by anatomical criteria, were applied by radiologists in order to ensure a correct delineation of the IFL.

3.6 Landmarks

Anatomical landmarks, defined by single voxel ROIs, were applied for co-registration of the tracks. This allowed for comparisons of diffusion parameters between corresponding segments of the pathways between the different groups. The number of landmarks was chosen based on the opportunities to localize anatomical points in a simple and rigorous way. Hence, the localization was done in an equal way as for the ROIs used to extract the WM pathay, based on anatomical definitions made by Catani *et .al.* and Mori *et. al.* Four separate landmarks were employed for the IFL and three separate landmarks were used for the IFO, see an example in Figure 8. The landmark in each slice was set to the position of the voxel showing the highest FA value within the track bundle, because this voxel presumed to have the highest certainty of tracks, corresponding to the reconstructed WM pathway, to pass.

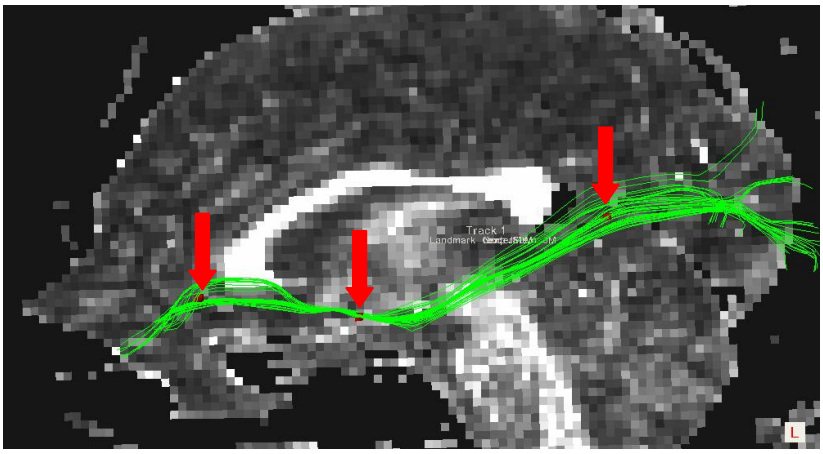

Figure 8 A typical IFO (in green) from one of the volunteers, visualised on a sagittal parametric FA-map. The three anatomical landmarks are shown in red, and are marked by the red arrows.

3.7 Algorithm

The tracks, calculated and produced by Trackvis, were imported into Matlab (Mathwords, Natick, Massachusetts, USA) and further processed using an in-house developed algorithm.

The first step in the algorithm was to calculate the mean track of all the tracks, which were described by consecutive points distanced by 1.0 mm, i.e. the tracks were defined by $[\mathbf{p}_i]_j$, where $[\mathbf{p}_i]_j$ is the *i*:th point in the *j*:th track. The calculation was performed according to the following procedure, described in steps A-G. (A) To start, the longest of the tracks was selected as a reference track. (B) The mid-point in the reference track, $[\mathbf{p}_x]_y$, was defined as the preliminary starting position of the mean track ($\mathbf{m}_0$*). (C) A preliminary normal vector ($\mathbf{v}_0$*) was calculated according to

$$\mathbf{v}_0^* = [\mathbf{p}_{x+1}]_y - [\mathbf{p}_x]_y \quad (5)$$

where $[\mathbf{p}_{x+1}]_y$ is the position of the next point in relation to $[\mathbf{p}_x]_y$ in the reference track. The length of $\mathbf{v}_0$* was then enforced to be unity. (D) Distances between the points in the individual tracks and a plane, with a normal $\mathbf{v}_0$*, that intersects $\mathbf{m}_0$* were calculated according to

$$[d_i]_j = \left| \left([\mathbf{p}_i]_j - \mathbf{m}_0^* \right) \cdot \mathbf{v}_0^* \right| \quad (6)$$

For each track *j*, the point with the shortest $[d_i]_j$ was selected. If $[d_i]_j$ < 1.5 mm, the point $[\mathbf{p}_i]_j$ was assumed to be within the cross section of the mean track. These points were denoted intersection points, $\mathbf{q}_k$, such that

$[\mathbf{q}_1, \mathbf{q}_2, \ldots, \mathbf{q}_m] = \{[\mathbf{p}_i]_j \mid [d_i]_j < 1.5 \text{ mm and } [d_i]_j = \min [d_{i=1..n}]_j \}$

These intersection points later contributed in the extraction of the diffusion parameters.

(E) The first position of the mean track ($\mathbf{m}_0$), replacing the preliminary $\mathbf{m}_0$*, was then calculated according to

$$\mathbf{m}_0 = \frac{1}{m} \sum_{k=1}^{m} \mathbf{q}_k \quad (7)$$

where *m* is the number of intersection points fulfilling the criteria in D. (F) A new normal vector $\mathbf{v}_0$ was calculated as the average of all vectors $\mathbf{u}_k = [\mathbf{q}_{i+1}]_k - [\mathbf{q}_i]_k$, i.e. the direction vectors of the tracks with points in the cross section, according to

$$\mathbf{v}_0 = \frac{1}{m}\sum_{k=1}^{m} u_k \tag{8}$$

(G) By taking a step forwarded along the direction of $\mathbf{v}_0$, the next position in the mean track was created according to

$$\mathbf{m}_{i+1} = \mathbf{m}_i + L\mathbf{v}_i \tag{9}$$

where the distance L was 1.5 mm. (H) The calculation of the mean track then proceeded iteratively, repeating steps D-G until the end of the tracks were reached. This procedure resulted in a mean track defined by points [$\mathbf{m}_0$, $\mathbf{m}_1$, …, $\mathbf{m}_n$], see Figure 9. Finally, a smoothing filter was applied to the mean track.

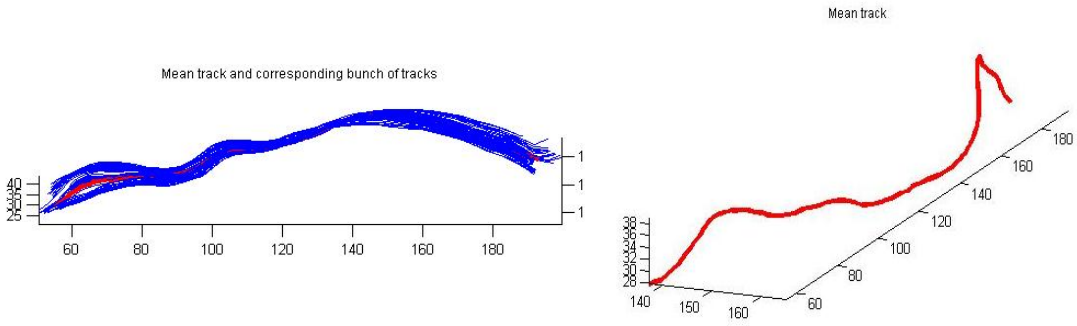

Figure 9 The individual tracks in a typical IFO are coloured in blue (left) and the resulting mean track is shown without the tracks (right). The tracks distribute in three dimensions and the axes correspond to track positions in the image coordinate system.

The next step was to co register the track bundles within a group. This was done by relating the mean track positions to the anatomical landmarks [$\mathbf{l}_1$, $\mathbf{l}_2$, …, $\mathbf{l}_m$], where m refers to the number of landmarks placed in the WM pathway. Distances between all points in the mean track and the landmarks were calculated for each landmark, according to

$$d_{ik} = \left|\mathbf{m}_i - \mathbf{l}_k\right| \tag{10}$$

where d_{ik} is the distance, i is the index of the mean track position and k is the landmark index. The points in the mean track that were closest to each of the landmarks were defined to represent the anatomical locations of those landmarks, i.e. $\mathbf{l}_k \approx [\mathbf{m}_i]_k$ so that $d_{ik} = \min d_{i=1..n,k}$. Consequently, the intervals between those points in the mean track were assumed to represent the same anatomical segments between all subjects in the group. The mean diffusion parameter values, in this example FA, were calculated along the segment between $\mathbf{l}_k$ and $\mathbf{l}_{k+1}$ according to

$$\mathrm{FA}(x) = \mathrm{c}\cdot\mathrm{FA}(\mathbf{m}_i) + (1-\mathrm{c})\cdot\mathrm{FA}(\mathbf{m}_{i+1}) \tag{11}$$

where x = [0,1) and

$$i = \lfloor x \cdot n_k \rfloor \tag{12}$$

with n_k being the number of points in the mean track and c defined as l/L, where $l = (i+1)L - x$. The values at different positions along the mean track, FA($\mathbf{m}_i$), were calculated as the mean parameter value of the intersection points, $\mathbf{q}_{k=1..m}$. Finally, the average and standard deviation of the parameters at each position along the segments were extracted for the different subjects and compared between the different groups. The parameter values representing the groups

were statistically significance tested with a non-parametric rank sum test at each position along the segments.

To estimate the cross-section areas along the track bundles, the covariance matrix of the intersection points in each cross section, cov($\mathbf{q}_{k=1..m}$), was calculated. The roots of the eigenvalues in each covariance matrix were used as the bases in an ellipse in the plane of the cross section. The area of the ellipse was denoted as the apparent area coefficient (AAC), and was treated in the same manner as the other diffusion parameters.

4. Results

Diffusion parameters for the different groups were plotted versus the position along the mean track, in an arbitrary scale, but with the distances between the anatomical landmarks scaled according to their average relative distance. Statistically significant differences in the parameter values between the two groups ($p < 0.05$) were marked by thick black lines slightly above the horizontal axis. The coloured areas above and below the plotted mean values corresponded to the standard deviations of the mean in each group. The plotted diffusion parameters were FA, MD, AAC and the eigenvalues λ_1, λ_2 and λ_3. The most anterior part of the IFO was not analysed in regard to AAC, because the track connections to the OFC are spatially very spread out, leading to extremely large values of the AAC.

4.1 Young Male – Female

The comparison between M/F showed quite similar parameter values in the two groups, which can be seen from Figure 10. There was a good agreement between the eigenvalues as well, mainly in the first and third ones, and the standard deviations were in the same order of magnitude as the standard deviations for FA and MD. In regard to group comparisons between the remaining groups, the value of the AAC was relatively large in the comparison between M/F which can be seen in Figure 10 A-F.

4.2 Young - Old

The comparison between Y/O showed significant differences in both anterior and posterior parts of the brain, see Figure 11. Trends of gradually increasing MD and λ_1 were observed in the anterior-to-posterior direction of the IFO, similar to what was observed in the comparison between young male and female. The values of λ_2 were slightly higher than the values of λ_3. The values of the AAC were in good agreement between the groups, except near the occipital lobe, where the AAC in the elderly group decreased while AAC in the younger group increased. However, this difference was not significant.

4.3 Semantic dementia patients – Healthy controls

The patients showed statistically significant evidence of lower FA and higher MD in the IFO, when compared with the controls. The largest differences in the FA values were observed around the central landmark. Between the central landmark and the occipital lobe, the FA values increased gradually. MD values were for patients most separated from HC near the occipital lobe. MD values in patients increased from the position of central landmark until the tracks reached the occipital lobe. Moreover, λ_1, λ_2 and λ_3 were significantly higher for some regions in the patients group than in the controls, with the largest difference in the posterior part of the brain, see Figure 12.

4.4 IUGR patients – Healthy controls

The comparison of diffusion parameters in the IFL between IUGR patients and HC showed significant differences of FA in positions near the second landmark of the IFL, and of MD in positions between the two first landmarks. The standard deviations were in the same order of magnitude in all analysed parameters, except for the AAC. The values of AAC were larger, with larger standard deviations, in HC compared to the values of AAC in patients, see Figure 13.

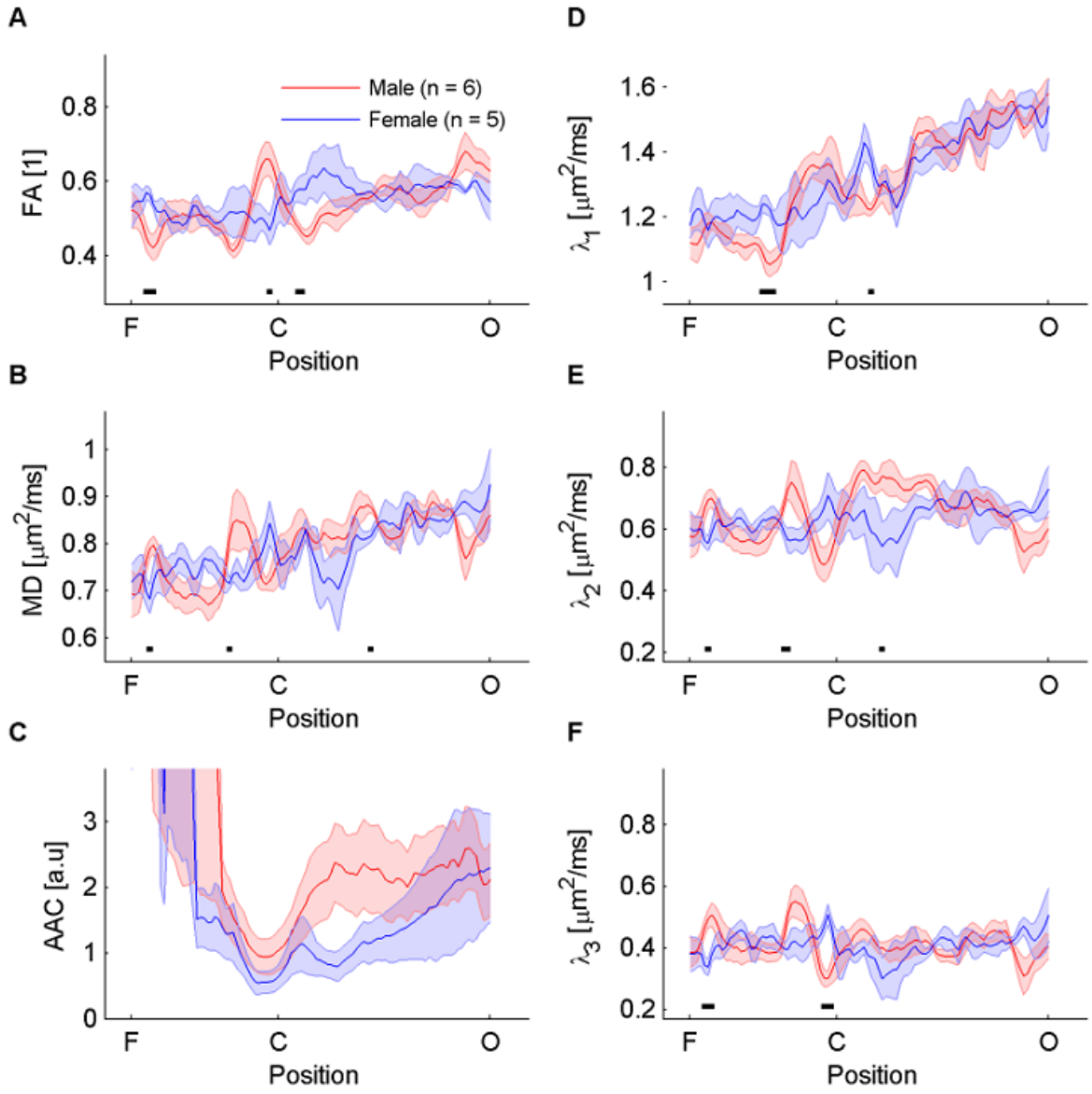

Figure 10 A-F. Comparison between diffusion parameters in groups of males (red) and females (blue) volunteers. Measurements from the group of males and females are shown in red and blue lines, respectively. The coloured area shows the standard deviation of the mean value in each position. The thick black lines slightly above the horizontal axis show the positions of significant differences between the groups. Panels A-F shows FA, MD, AAC and the eigenvalues along the positions of the IFO.

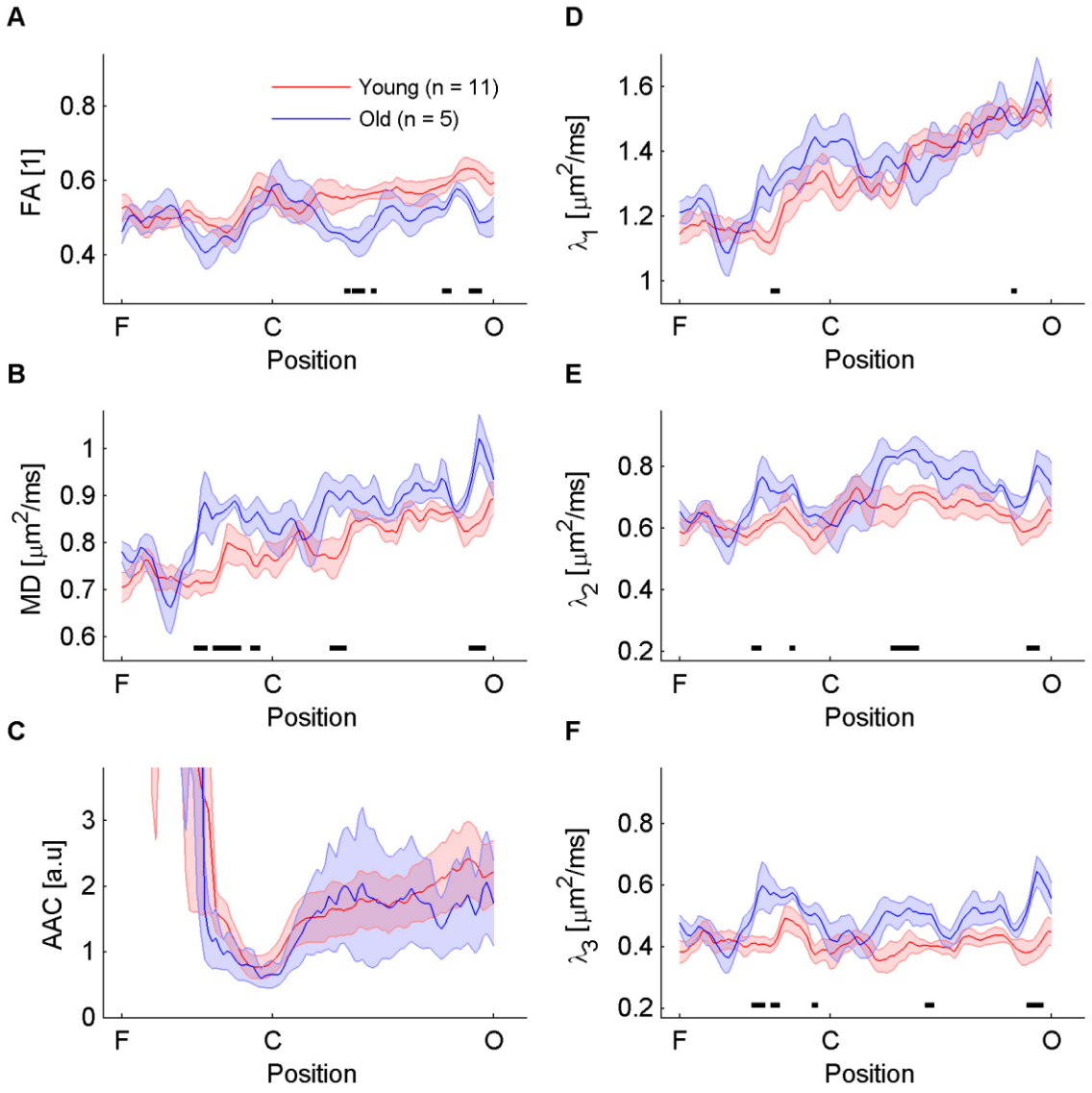

Figure 11 A-F. Comparison between diffusion parameters in groups of young (red) and old (blue) volunteers. The coloured area shows the standard deviation of the mean in each position. The thick black lines slightly above the horizontal axis show positions of significant differences between the groups. Panels A-F shows the FA, the MD, the AAC and the eigenvalues along the positions of IFO. The parameter values varied slightly along the IFO, and in some regions the parameter values were significantly different, except for the AAC.

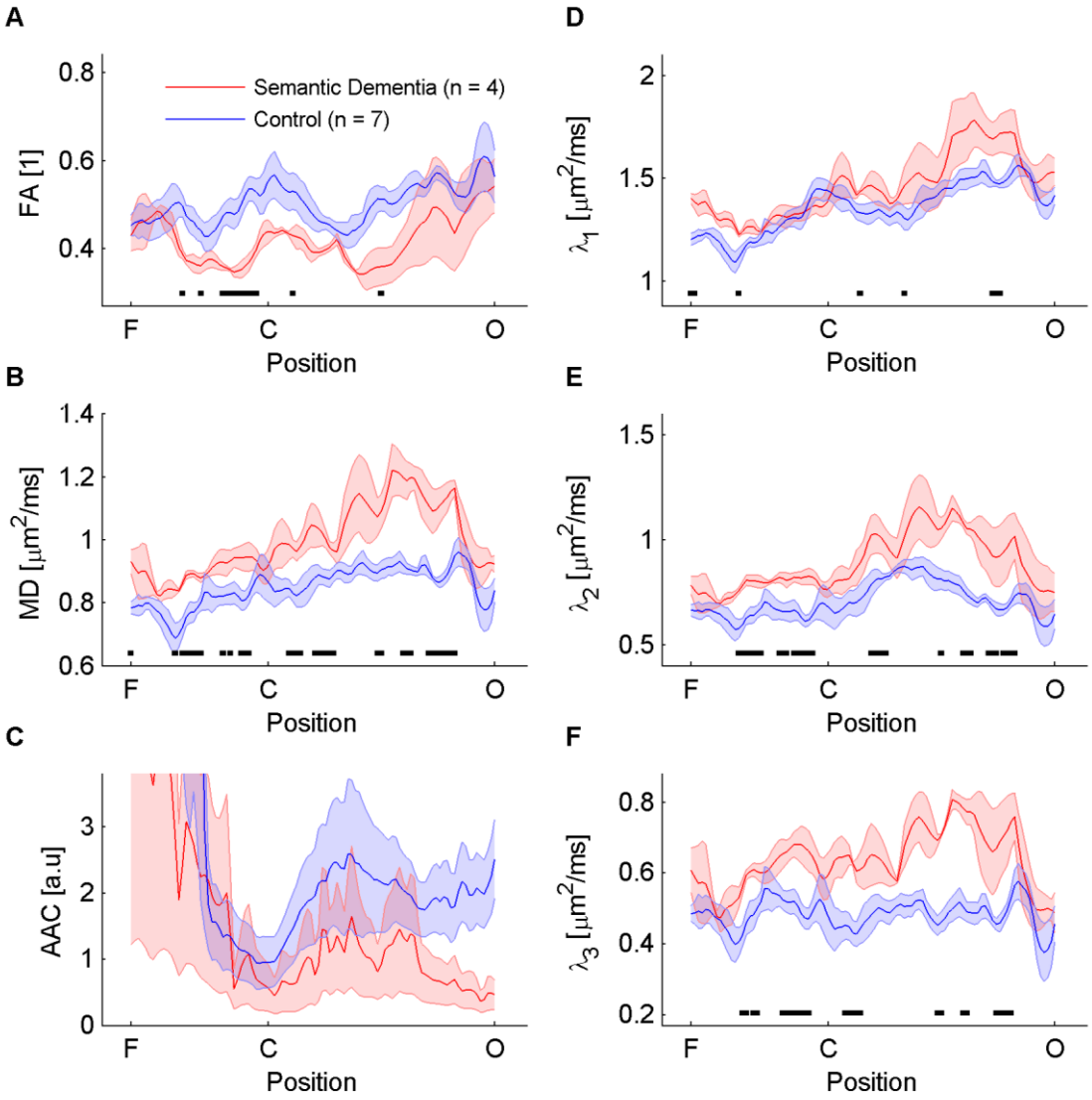

Figure 12 A-F. Comparison between diffusion parameters and the AAC in groups of patients suffering from SD (red) and HC-SD (blue) volunteers. The coloured area shows the standard deviation of the mean in each position. Panels A-F shows FA, MD, AAC and the eigenvalues along the positions of the IFO.

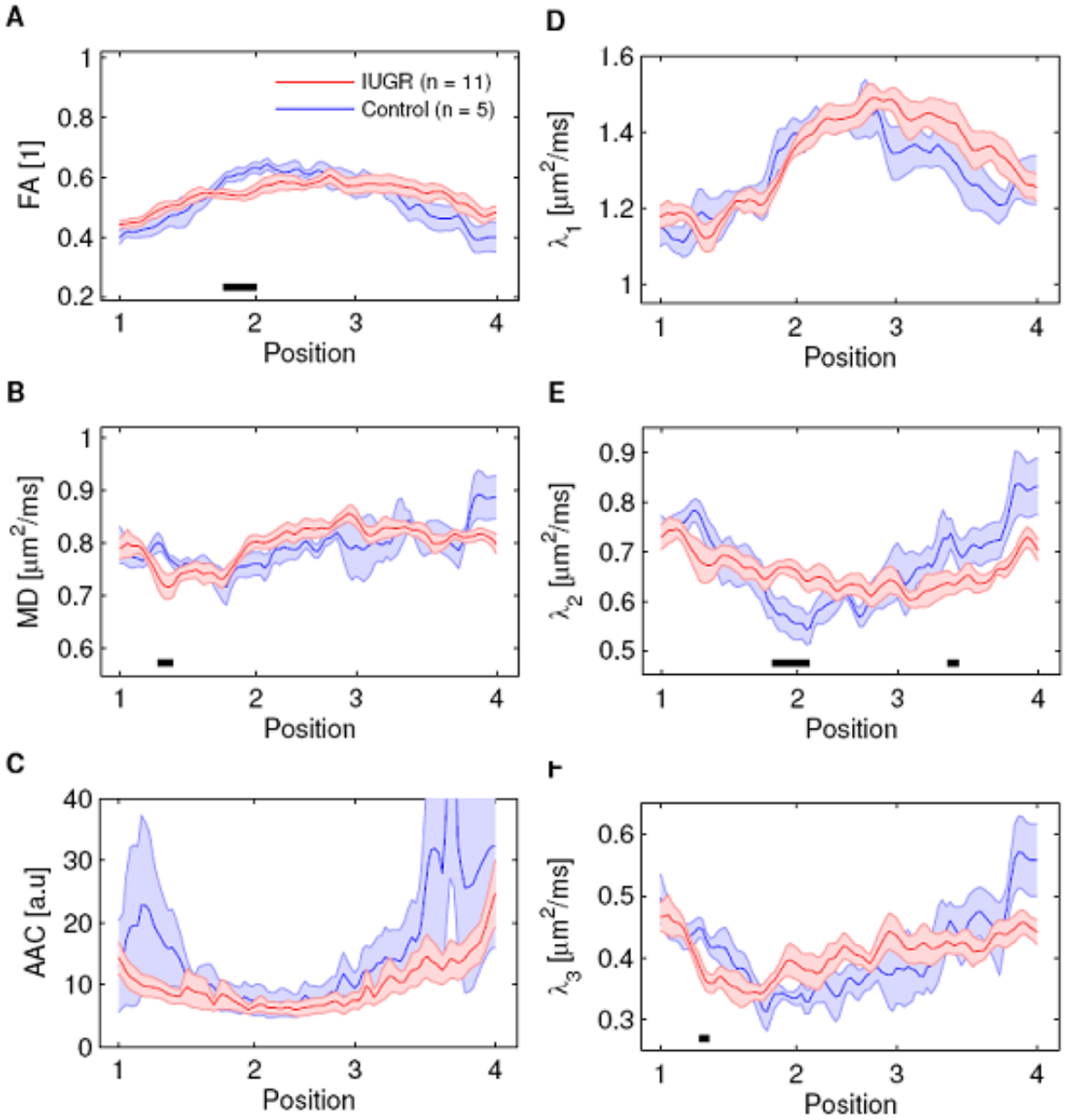

Figure 13 A-F. Comparison between diffusion parameters and the AAC in groups of patients suffering from IUGR (red) and HC-IUGR (blue) volunteers. The coloured area shows the standard deviation of the mean in each position. Panels A-F shows FA, MD, AAC and the eigenvalues along the positions of the IFL.

5. Discussion

In present work, a new analysis method for quantifying diffusion parameters along WM pathways was developed. The method was applied to perform group comparisons in order to find regional differences. Significant regional differences were observed, for example, in the comparison between IUGR patients and HC-IUGR, see Figure 13. Such a difference was not previously found when the data was analysed using conventional tractography methods, where only one average parametric value was calculated for each track bundle and then compared between the patient and control group.

The results from the group comparisons between Y/O and M/F both corresponded to what was expected from previous studies, see Figure 10 and Figure 11 [48,49,50]. In the Y/O comparison, the younger age interval was chosen to fit the peak in anisotropic diffusion, which appears in the middle age when the myelination reaches its maximum [48]. The observed significant differences in diffusion properties between young and elderly were primarily found in the frontal lobe for the FA values and in the occipital lobe for the MD values. It would, however, be interesting to further investigate why the parameters were significantly different at those specific positions of the IFO and if the changes appeared due to demyelination or to a larger amount of crossing fibres as discussed in the introduction. The ages in the young group were more homogeneous than in the elderly group, i.e. the standard deviations in ages were 2.0 y and 6.6 y, respectively. In further investigations, it would be beneficial to include larger and more age-similar groups. The significant differences that were observed in a few positions in the comparison between the genders, see Figure 10, were likely false positives. The final result may contain 5% false positives, i.e. false significant differences in the parameter values, according to the statistical non-parametric rank sum test with a significance level of 0.05. As a conclusion from the comparisons between different groups among the healthy controls, the results corresponded to what was expected, which served as a basic validation of the algorithm.

Subjects in the HC-SD group were tested in regard to semantic memory and neurological capacity by an experienced neurophysiologist before they were included in the study. This was done in order to exclude confounders from the study. Decreasing FA values was correlated to increasing MD values, which could be an indication of higher diffusivity in a direction perpendicular to the analysed tracks. Both the FA and the MD as well as the second and the third eigenvalues showed significant differences between the two groups in the frontal lobe, see Figure 12. The observed differences could potentially be used as a step in the early diagnosis of dementia.

The IUGR study included subjects in the age interval 23 – 25 y, which means that a long time had elapsed since their premature birth. The reason to this was that cognitive and neurological symtoms often affect IUGR patients later in life. The clinical question in this case was to evaluate whether or not deviations in diffusion properties of the IFL could explain the cognitive and neurological symtoms in grown up IUGR patients. The contiguous regions with significant different diffusion properties implied that the IFL is affected in these patients.

Tractography has previously been used for analysing diffusion parameters along WM pathways. Few of these methods have been applied to the IFO or the IFL, which were of interest in the clinical question at issue and many of the WM pathways that have been analysed differ in their spatial extent from the IFO and the IFL. In addition, none of the performed studies, to the best of our knowledge, performed a co-registration between the track bundles as extensive as it was made in this work.

A limitation of the present study was that the diffusion tensor was employed in the tractography. The quality of the tractography depends on the amount of crossing fibers, which is a limitation arising from the assumption about the Gaussian diffusion in the diffusion tensor approximation. The tensor model is thus not able to resolve multiple fibre orientations within voxels, i.e. crossing fibers [51]. The result then becomes affected by increased diffusivity in the perpendicular directions to the WM pathway. The MD increases and the FA decreases in those positions due to the crossing fibers. In voxels with FA-values below the threshold of 0.2, the tracking was terminated. Consequently, crossing fibres can interrupt the tracking. If the tractography was used to diagnose diseases, this would be able to impair the quality of the evaluation.

The algorithm developed in this study includes user dependent steps that are not automatically performed in the tractography calculation. One of them is the positioning of the ROIs, which is performed manually. In this process, it is of outmost importance to consequently follow anatomical definitions of where the pathway passes. The extracted track bundles can nevertheless be affected by other WM pathways [51] and therefore these must be excluded in a consequent manner [39, 45, 46].

Positioning of the landmarks was another user-dependent step and the accuracy in those placements should be evaluated in a separate study. For instance, the inter-observer reproducibility of the landmark positioning could be investigated. However, the landmarks made the method usable for patients with atrophy, which is often present in dementia patients, since conventional image co registration is difficult in that case. For patients suffering from IUGR, measurements can be repeated at different ages without the method being sensitive to the anatomical differences in the size of the brain.

The capability of the AAC parameter to characterize pathways is not yet satisfying and the calculation of this parameter could be further developed. However, the parameter can be useful to inform the user about the spatial extension of the track bundle. Similar metrics have not been seen in the literature by the author. The parameter can preferable be used together with information about the number of analysed tracks. Few tracks with high AAC can be an indication of spatially highly spread-out tracks, while lots of tracks together with a small value of AAC can be an indication of a high density of tracks. This could be of interest to study in group comparisons where the WM pathway in one of the groups is expected to be thin due to WM degeneration. Another parameter of interest, for instance in cases where the anatomy is expected to be affected, would be the quantified spatial shape of the WM pathway.

In conclusion, the information provided in this method is valuable for several clinical questions at issue. The in vivo results showed that significant differences in regions along WM pathways can be found using this analysis method. The method consequently shows potential to be valuable to future clinical research projects.

Acknowledgments

I would like to thank my supervisors, **Jimmy Lätt** and **Markus Nilsson**, for all invaluable help and support and that you gave me during this exciting time. Thanks for all the patience you showed and the knowledge you shared with me. It is a pleasure to work with you.

I would also like to thank my cooperators during my way; **Henrik Hansson** for worthwhile discussions about Matlab and a great company in Kitzbuhel**, Danielle van Westen** for advising and sharing your anatomical knowledge, **Christina Elfgren** and **Christer Nilsson** for valuable discussions and ideas, **Isabella Björkman-Burtscher** and **Anna Kahn** for contributions and help in many ways, and to all the members of the **MR physics group in Lund**, who believed in me and made me feel welcome in the group.

Last but not least I want to thank my **family** for their infinite support during my education; it would not have been possible without you. Thanks to my gorgeous daughter, **Isabell**, for your interest and never-ending patience, I love you.

References

1 Lätt J. Investigation of Water Mobility using Diffusion-Sensitive MRI: The Role of q-Space Imaging, High b-Values and Diffusion Time. ISBN 978-91-628-7413-1. 2008

2 Lätt J, Nilsson M, van Westen D, Wirestam R, Ståhlberg F, Brockstedt S. Diffusion-weighted MRI measurements on stroke patients reveal water-exchange mechanisms in sub-acute ischemic lesions. NMR in Biomedicine 2009; 22(6): 619-628

3 Le Bihan D, Turner R, Douek P, Patronas N. Diffusion MR imaging: Clinical Applications. American Journal of roentgenology. 1992; 159: 591-599

4 Lehmann C H, Zhang J, Mori S, Sheikh K A. Diffusion tensor imaging to assess axonal regeneration in peripheral nerves. Experimental Neurology 2010; 223: 238–244

5 Coremans J, Luypaert R, Verhelle F, Stadnik T, Osteaux M. A method for myelin fiber orientation mapping using diffusion-weighted MR images. Magnetic Resonance Imaging 1994; 12(3): 443-454

6 Jones D. Determining and Visualizing Uncertainty in Estimates of Fiber Orientation From Diffusion Tensor MRI. Magnetic Resonance in Medicine 2003; 49: 7–12

7 Wakana S, Jiang H, Nagae-Poetscher van Zijl CM, Mori S. Fiber Tract-based Atlas of Human White Matter Anatomy. Radiology 2004; 230: 77–87

8 Mori S, Wakan S, Nagae-Poetscher LM, van Zijl PCM. ISBN:0444517413 Elsevier Science 2005

9 Faria V A, Oishi K, Mori S. Study of White Matter Anatomy and 3D Tract Reconstruction by Diffusion Tensor Imaging Inc. International Journal of Imaging System Technology 2010; 20: 51–56

10 Giorgio A, Watkins KE, Chadwick M, Winmill J, Douaud G, De Stefano N, Matthews PM, Smith SM Johansen-Berg H, James AC. Longitudinal changes in grey and white matter during adolescence. NeuroImage 2010; 49: 94–103

11 Rose E S, Janke L A, Chalk B J. Gray and White Matter Changes in Alzeimer´s Disease: A Diffusion Tensor Imaging Study. Journal of magnetic imaging 2008;27: 20-26

12 Shiee N, Bazin P-L, Ozturk A, Reich D, Calabresi P A, Pham D L. A topology preserving approach to the segmentation of brain images with multiple sclerosis lesions. NeuroImage 2010; 49(2): 1524-1535

13 Mao P, Reddy P H. Is multiple sclerosis a mitochondrial disease? Biochimica et Biophysica Acta 2010;1802: 66-79

14 Ihara M, Polvikoski M T, Hall R, Slade Y J, Perry H R, Oakley E A, Englund E, O'Brien T J, Ince G P, Kalaria N R. Quantification of myelin loss in frontal lobe white matter in vascular dementia, Alzheimer's disease, and dementia with Lewy bodies. Acta Neuropathology 2010; 119: 579-589

15 Bartzokis G. Age-related myelin breakdown: a developmental model of cognitive decline and Alzheimer's disease. Neurobiology of Aging 2004; 25: 5-18

16 Meyer J S, Kawamura J, Terayama Y. White matter changes in the elderly. Journal of the neurological sciences 1992; 110: 1-7

17 Takahashi E, Dai G, Wang R, Ohki K, Rosen G, Galaburda A M, Grant P E, Wedeen Van J. Development of cerebral fiber pathways in cats revealed by diffusion spectrum imaging. NeuroImage 2010;49: 1231-1240

18 Betarbet R, Canet-Aviles R M, Canet-Aviles T B, Mastroberardino P G, McLendon C, Kim J-H, Lund S, Na H-M, Taylor G, Bence N F, Kopito R, Boo Seo B, Yagi T, Yagi A, Klinefelter G, Cookson M R, Greenamyre J T. Intersecting pathways to neurodegeneration in Parkinson's disease: Effects of the pesticide rotenone on DJ-1, A-synuclein, and the ubi-quitin–proteasome system. Neurobiology of Disease 2006; 22: 404-420

19 Susumu Mori S, Frederiksen K, van Zijl P CM, Stieltjes B, Kraut M A, Solaiyappan M, Pomper M G. Brain White Matter Anatomy of Tumor Patients Evaluated with Diffusion Tensor Imaging. Annals of Neurology 2002; 53(2): 377-380

20 Gerig G, Gouttard S, Corouge I. Analysis of Brain White Matter via Fiber Tract Modeling. IEEE EMBS 2004

21 Pievani M., Agosta F, Pagani E, Canu E, Sala S, Absinta M, Geroldi C, Ganzola R, Frisoni G B, Filippi M. Assessment of white matter tract damage in mild cognitive impairment and Alzheimer's disease. Human Brain Mapping, n/a. doi: 10.1002/hbm.20978, 2010

22 Mojtaba Zarei M, Patenaude B, Damoiseaux J, Morgese C, Smith S, Matthews PM, Barkhof F, Rombouts S, Sanz-Arigita E, Jenkinson M. Combining shape and connectivity analysis: An MRI study of thalamic degeneration in Alzheimer's disease. NeuroImage 2010; 49(1): 1-8

23 Duffau H, Thiebaut de Schotten M, Mandonnet E. White matter functional connectivity as an additional landmark for dominant temporal lobectomy. Journal of Neurology Neurosurgery and Psychiatry 2008; 79: 492-495

24 Catani M, Thiebaut de Schotten M. A diffusion tensor tractography atlas for virtual in vivo dissections. Cortex 2008: 2-4, 7-14, 26-32

25 Tideman E, Marsál K, Ley D. Cognitive function in young adults following intrauterine growth restriction with abnormal fetal aortic blood flow. Ultrasound in Obstetrics and Gynecology 2007; 29(6): 614-618

26 Le Bihan D, Breton E, Lallemand D, grenier P, Cabanis E, Laval-Jeantet M. MR imaging of intravoxel incoherent motions: application to diffusion and perfusion in neurologic disorders. Radiology 1986: 161: 401-407

27 Moseley ME, Cohen Y, Mintorovitch J, Chileuitt L, Shimizu H, Kucharczyk J, Wendland MF, Weinstein PR. Early detection of regional cerebral ischemia in cats: Comparison of diffusion- and T2-weighted MRI and spectroscopy. Magnetic resonance in Medicine 1990; 14: 330-346

28 Basser P J, Matiello J, Le Bihan D. MR diffusion tensor spectroscopy and Imaging. Biophysics Journal 1994; 66: 259-267

29 Fillard P, Gilmore J, Piven J, Lin W, Gerig G. Quantitative Analysis of White Matter Fiber Properties along Geodesic Paths. Elseviewer science 2004; 2-11

30 Savannah C. Partridge S C, Mukherjee P, Berman J I, Henry R G, Miller S P, Lu Y, Glenn O A, Ferriero D M, Barkovich J, Vigneron D B. Tractography-Based Quantitation of Diffusion Tensor Imaging Parameters in White Matter Tracts of Preterm Newborns. Journal Of Magnetic Resonance Imaging 2005; 22: 467–474

31 Klein J, Hermann S, Konrad O, Hahn HK, Peitgen H-O. Automatic Quantification of DTI Parameters along Fiber Bundles. ISBN978-3-540-710912 SpringerLink 2007: 272-276

32 Brown R. A brief account of microscopical observations on the particles contained in the pollen of plants; and on the general existence of active molecules in organic and inorganic bodies. 1827

33 Einstein A. On the Movement of Small Particles Suspended in Stationary Liquids Required by the Molecular-Kinetic Theory of Heat. Annalen der Physik 1905; 17(4): 549–560. , 1905

34 Faria A, Oishi K, Mori S. Study of White Matter Anatomy and 3D Tract Reconstruction by Diffusion Tensor Imaging. Inc. International Journal of Imaging Systems and technology 2010; 20: 21-56

35 Scarabino T, Salvoni U, Salle Di F, Duvernoy H, Rabischong P. Atlas of morphology and functional anatomy of the brain. ISBN13978-3-540-29628-7 Springer Berlin Heidelberg, Germany, 2006

36 Meerwall von E, Ferguson R.D. Interpreting pulsed-gradient spin echo diffusion experiments with permeable membranes. Journal of chemistry physics 1981; 74(12)

37 Horsfield M A, Jones D K. Applications of diffusion weighted and diffusion tensor MRI to white matter diseases – a review. NMR Biomedicine 2002; 15: 570-577

38 Hsu J-L, Van Hecke W, Bai C-H, Lee C-H, Tsai Y-F, Chiu H-C, Jaw F-S, Hsu C-Y, Lau J-G, Chen W-H, Leemans A. Microstructural white matter changes in normal aging: A diffusion tensor imaging study with higher-order polynomial regression models. NeuroImage 2010; 49: 32-43

39 Scarabino T, Salvolini U. Atlas of morphology and functional anatomy of the brain. Springer Berlin Heidelberg. Germany, 2006

40 Schroeter ML, Raczka K, Neumann J, Yves von Cramon D. Towards a nosology for frontotemporal lobar degenerations-a meta-analysis involving 267 subjects. Neuroimage 2007; 36(3): 497-510

41 Peleg D, Kennedy CM, Hunter SK. Intrauterine Growth Restriction: Identification and Management. American Academy of Family Physicians 1998.

42 Wang R, Wedeen Van J, Athinoula A. Martinos Center for Biomedical Imaging, Massachusetts General Hospital, Boston, MA 2007-2010

43 Jenkinson M, Smith S.M. A global optimisation method for robust affine registration of brain images. Medical Image Analysis 2001; 5(2): 143-156

44 Wang R, Wedeen Van J, Athinoula A. Martinos Center for Biomedical Imaging, Massachusetts General Hospital, Boston, MA 2007-2010.

45 Faria A V, Oishi K, Mori S. Study of white matter anatomy and 3D tract reconstruction by diffusion tensor imaging. International journal of systems and technology 2010; 20: 51-56

46 Catani M, Thiebaut de Schotten M. A diffusion tensor tractography atlas for virtual in vivo dissections. Cortex 2008: 2-4, 7-14, 26-32

47 Kier E L, Staib L H, Davis L M, Bronen R A. MR Imaging of the Temporal Stem: Anatomic Dissection Tractography of the Uncinate Fasciculus, Inferior Occipitofrontal Fasciculus, and Meyer's Loop of the Optic Radiation. American Journal of Neuroradiology 2004; 25: 677–691

48 Hsu J-L, Van Hecke W, Bai C-H, Lee C-H, Tsai Y-F, Chiu H-C, Jaw F-S, Hsu C-Y, Leu J-G, Chen W-H, Leemans A. Microstructural white matter changes in normal aging: A diffusion tensor imaging study with higher-order polynomial regression models. NeuroImage 2010; 49: 32-43

49 Giorgio A, Watkins K E, Chadwick M, James S, Winmill L, Douaud G, DeStefano N, Matthews P M, Smith S M, Johansen-Berg H, James A C. Longitudinal changes in grey and white matter during adolescence. Neuroimage 2010; 49: 94-103

50 Giorgio A, Watkins K E, Chadwick M, James S, Winmill L, Douaud G, De Stefano N, Matthews P M, Smith S M, Johansen-Berg H, James A C. Longitudinal changes in grey and white matter during adolescence. Neuroimage 2010; 49: 94-103

51 Mori S, van Zijl C M. Fiber tracking: principles and strategies - a technical review. NMR in biomedicine 2002; 15: 468-480